Role of electrochemical cell configuration on the selectivity of CuZnAl-oxide-based electrodes for the continuous CO2 conversion: aqueous electrolyte vs. catholyte-less

Discover Chemical Engineering

Research

Role of electrochemical cell configuration on the selectivity of CuZnAl-oxide-based electrodes for the continuous CO_2 conversion: aqueous electrolyte vs. catholyte-less configuration

Hilmar Guzmán[1,2] · Jonathan Albo[3] · Angel Irabien[3] · Micaela Castellino[1] · Simelys Hernández[1]

Received: 21 January 2024 / Accepted: 5 June 2024
Published online: 13 June 2024

Abstract
This research is a significant step forward in understanding how the electrochemical cell setup influences CO_2 conversion. The performance of Cu–Zn–Al metal oxide-based catalysts was compared in two reactor configurations: a gas diffusion electrode (GDE) cell with an aqueous electrolyte and a Membrane Electrode Assembly (MEA) cell operating in the gas phase without catholyte. The different operations induced significant morphological and crystalline structural changes, profoundly impacting the catalytic behaviour. The MEA configuration, for instance, led to the formation of a higher Cu^0/Cu^{1+} ratio in the catalysts, promoting C–C coupling for C_2H_4 production. Conversely, the GDE operation favoured alcohol (ethanol and methanol) production by balancing copper oxidation states formed in situ in the presence of the aqueous catholyte. Zn and Al oxides also played a role in stabilising the resulting Cu species, some of which remained oxidised on the electrode surface. These findings underscore the crucial influence of varying cell operation conditions on catalyst reconstruction, shaping the quantity of $Cu^0 + Cu^{1+}$ species formed in situ to tailor catalyst selectivity.

Keywords Copper oxide · Zinc oxide · Alumina · Gas diffusion electrode · Catholyte-less conditions · CO dimerisation · C_{2+} products · Electrochemical CO_2 reduction

1 Introduction

Reducing greenhouse gas (GHG) emissions to combat climate change is one of the toughest challenges in recent years [1]. Despite increasing pressure to cut emissions, they remain alarmingly high, especially from the energy sector, the primary source of global CO_2 emissions. Electrochemical CO_2 reduction (EC CO_2R) holds promise for mitigating these emissions and achieving carbon neutrality [2]. However, CO_2 stability presents a hurdle, requiring significant energy input to overcome kinetic barriers [3, 4]. While CO and formic acid are the primary focus of EC CO_2R research due to their simplicity, there is growing interest in producing more complex carbon products like C_2H_4, driven by its substantial market demand [5]. According to the Precedence Research company, the global C_2H_4 market size was USD 176 billion in 2021.

Hilmar Guzmán and Jonathan Albo contributed equally to this work as first authors.

Supplementary Information The online version contains supplementary material available at https://doi.org/10.1007/s43938-024-00049-6.

✉ Simelys Hernández, simelys.hernandez@polito.it | [1]CREST Group, Department of Applied Science and Technology (DISAT), Politecnico di Torino, C.so Duca degli Abruzzi, 24, 10129 Turin, Italy. [2]IIT, Istituto Italiano di Tecnologia, Via Livorno, 60, 10144 Turin, Italy. [3]Departamento de Ingenierías Química y Biomolecular, Universidad de Cantabria, Avda. Los Castros s/n, 39005 Santander, Spain.

It is expected to surpass around USD 287 billion by 2030, and it is anticipated to reach a registered Compound Annual Growth Rate (CAGR) of 5.58% from 2022 to 2030 [6]. C_2H_4 is predominantly sourced from fossil fuels, highlighting the need for sustainable alternatives like EC CO_2R. The choice of electrocatalyst is crucial for optimising CO_2 conversion, with copper-based catalysts showing promising results [7, 8]. Operating in highly alkaline environments improves conductivity and reaction kinetics [9], but challenges such as carbonate salt formation and electrolyte stability persist. Neutral electrolytes offer a potential solution but face efficiency issues [10]. Moreover, downstream separation costs increase due to product dilution in large electrolyte volumes. Addressing these challenges and ensuring electrolyte stability is essential for developing an effective industrial EC CO_2R system.

One of the practical limitations of EC CO_2R technology is the low solubility of CO_2 in aqueous electrolytes (~ 38 mM at 20 °C and ambient pressure), hindering mass transport to the electrode surface. In this regard, porous electron conductive substrates are proposed to prepare electrodes and practical electrolyser designs to deal with CO_2 solubility and mass transport issues. Gas-diffusion electrodes (GDEs) enhance CO_2 concentration at electrode active sites, which is crucial for promoting multicarbon molecule synthesis [3]. The electrolyte can be aqueous to form a triple-phase (solid–liquid-gas) interface between the absorbed CO_2 and the catalyst/liquid electrolyte. It can also be an ion-conductive polymer transporting charged species (e.g., H^+) and forming a catalyst/polymer electrolyte interface with the absorbed CO_2 (see Fig. 1). By impregnating quaternary ammonia poly (ether ether ketone) ionomer into the porous Cu cathode, recent advancements have shown promising results in C_2H_4 synthesis, reaching approximately a Faradaic efficiency (FE) of 32% [11]. Catholyte-free EC CO_2R cell designs (zero-gap), where an ion-conductive polymer electrolyte is assembled with a GDE, are gaining attention for their compactness, energy efficiency, and reduced internal losses, but further improvements are needed to overcome challenges such as the dominance of the hydrogen evolution reaction (HER) at high current densities [12–19].

In the thermocatalytic hydrogenation of CO_2, amphoteric metal oxides (i.e. Al_2O_3, ZnO) support and stabilise Cu nanoparticles. Al_2O_3 is widely explored as a catalyst support for methanol production at industrial scales [20] and has been applied in CO_2 co-electrolysis for value-added product generation. Combining ZnO and Al_2O_3 with Cu-based electrocatalysts has enhanced catalytic performance, achieving high FE for syngas ($CO + H_2$) production in a batch CO_2-dissolved liquid-phase electrochemical cell under ambient conditions [21]. CuZn materials are gaining attention as electrocatalysts due to their low cost and environmental friendliness. The addition of Zn into the Cu electrode is expected to inhibit the H_2 formation due to the low activity of Zn toward the HER and to increase the local concentration of *CO intermediate since Zn is a CO-generation catalyst, which may help to stabilise the Cu^{1+} species in the hydrogenation reaction [22–24]. In fact, some of us recently demonstrated by ex-situ characterisation that the presence of ZnO nanoparticles in mixed Cu/ZnO catalysts plays an essential role in the formation and stabilisation of mixed oxidation states of copper (Cu^{1+} and Cu^0) in the electrocatalyst, after a batch EC CO_2R with a CO_2-saturated electrolyte. The local amount of *CO intermediates seemed to be enhanced as the mixed oxidation states increased. The relative amount depended on the applied potential, promoting the further dimerisation of *CO intermediates to generate C_{2+} products under ambient conditions [4]. Likewise, some of us observed that Cu oxides/ZnO-based surfaces enhance selectivity to C_2H_4 working in a continuous flow electrochemical cell, reaching a FE of 91% and a production rate of 487.9 $\mu mol \cdot m^{-2} \cdot s^{-1}$ under electrolyte-less conditions

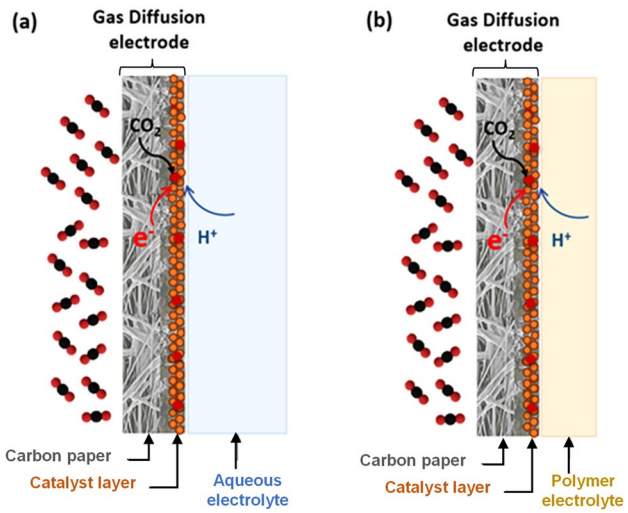

Fig. 1 Different reactor schemes for the EC CO_2R. Gas-fed CO_2R; in the presence of (**a**) a GDE and bulk aqueous electrolyte and (**b**) a membrane electrode assembly (MEA) with a GDE and a polymer electrolyte membrane (zero-gap)

[25]. The same electrocatalyst performed differently depending on the operating conditions during the electrocatalytic reactions [2, 4, 21]. The presence or absence of the liquid catholyte influences the diffusion and concentration of CO_2 on the electrode surface, forming different products. However, until now, there are no clear explanations for those differences in the literature.

This study investigates the impact of CuZnAl-based electrodes on the selectivity, FE, and production rate of carbon-based molecules during continuous EC CO_2R. Two cell configurations are compared: the conventional GDE setup utilising a liquid-phase bulk electrolyte and a catholyte-less zero-gap MEA configuration. Thus, GDEs and MEAs were fabricated, and electrochemical measurements were performed alongside ex-situ characterisation. Our results revealed that the catalytic activity and selectivity of the electrodes are primarily dictated by the contact between the components in the different configurations, thereby mass-transfer resistances, in addition to the inherent properties of the fresh electrocatalytic materials. According to our knowledge, this is the second attempt in the literature to assess the effect of different reactor conditions and electrode designs to maximise the performance of the continuous gas-phase EC CO_2R technology, evaluating the effect of electrocatalyst reconstruction [26]. Notably, we integrated the principles of gas-phase heterogeneous catalysis into electrocatalysis, evaluating the influence of stable metal oxide catalysts (such as ZnO and Al_2O_3) on promoting C–C coupling, both in the presence and absence of a liquid electrolyte. This approach extends beyond previous investigations on Cu oxidation states coupled to other metal oxides in batch liquid-phase systems.

2 Materials and methods

2.1 Preparation of CuZnAl-based electrodes

CuZnAl-based catalysts were prepared using a co-precipitation method previously described in detail. [21] Herein, three different materials with varying amounts of Cu, Zn, and Al were investigated: CuZA-06-03-01, CuZ-06-03 and Cu-06 (see Table 1). In brief, they were synthesised using solutions of hydrated metal nitrates ($Cu(NO_3)_2$, $Zn(NO_3)_2$, $Al(NO_3)_3$) as precursors and Na_2CO_3 (1 M) as precipitating agent. For the sake of clarity, for example, the name of CuZA-06-03-01 material stands for the CuO, ZnO, and Al_2O_3 composition and the concentration: Cu:Zn:Al = 0.6 M:0.3 M:0.1 M of the abovementioned metal nitrates. The CuZ-06-03 catalyst was obtained using the same precursor concentrations but deprived of Al (Cu:Zn = 0.6 M:0.3). Finally, the Cu-06 material was prepared using a $Cu(NO_3)_2$ 0.6 M solution.

A previous work meticulously detailed all the information concerning the physical–chemical characterisation of the pristine materials [21]. Electrodes were manufactured by airbrushing a catalytic ink on a porous carbon support (Toray carbon paper, thickness 0.19 mm Teflon 20 (±5) wt % treated, Quintech) with a microporous layer (MPL). The catalytic ink was composed of i) the CuZnAl-based powders (as the electrocatalytic material), ii) Nafion dispersion, 5%wt in water and 1-propanol by Sigma Aldrich as the binder, and iii) isopropanol (99% of purity, Sigma Aldrich) as the liquid carrier. A Catalyst:Nafion ratio of 70:30 was kept for the electrode manufacturing to promote efficient reactant transport and good catalytic layer stability, whereas an isopropanol/solids mass ratio of 97:3 was used to ensure the catalyst dispersion. The MPL was constituted of Vulcan carbon powder (VXC72R, Cabot, carbon black) and polytetrafluoroethylene, PTFE (Sigma-Aldrich, 60 wt% dispersion in H_2O) with a 70:30 Vulcan/PTFE mass ratio. The electrodes were prepared with a geometric area of 10 cm^2 and a catalyst loading of 0.5 mg cm^{-2}. Then, the CuZnAl-based electrodes were assembled with the ion-conductive membrane (Nafion 117) at 50 °C and a pressure of 80 bar for a few minutes to develop a MEA (zero-gap) electrode using a filter press (Carver, Inc.).

Table 1 Composition of the prepared ternary catalysts

Sample	Precursor concentration, M			Main composition after calcination
	$Cu(NO_3)_2.3H_2O$	$Zn(NO_3)_2.6H_2O$	$Al(NO_3)_3.9\ H_2O$	
CuZA-06-03-01	0.6	0.3	0.1	$CuO/ZnO/Al_2O_3$
CuZ-06-03	0.6	0.3	–	CuO/ZnO
Cu-06	0.6	–	–	CuO

2.2 Electrocatalytic CO_2 reduction tests

The continuous flow electrochemical experiments were performed in a commercial Micro Flow Cell (ElectroCell*)*. It includes different spacers, gaskets, and end plates, where the pathways for the streams can be defined depending on the configuration. Here, two different configurations were explored to evaluate the prepared CuZnAl-based electrode performances: GDE and MEA. In the former, the cell was divided into three compartments: gas, catholyte and anolyte (see Fig. 2). The airbrushed electrodes were exploited as the working electrode (cathode), which is exposed on one side to the catholyte and, on the other side, to the CO_2 gaseous stream. A Nafion 117 cation exchange membrane (0.18 mm), previously activated, separated the catholyte and anolyte compartments to allow the selective transport of H^+ ions towards the cathode chamber. A platinised titanium plate was used as the counter electrode (anode), and an Ag/AgCl (sat. KCl) as the reference electrode. The gas compartment of the reactor was fed with CO_2 gas (99.99%) with a flow/area ratio equal to $Q_g/A = 18$ ml min^{-1} cm^{-2}, adjusted by a rotameter. The catholyte and anolyte, 0.5 M $KHCO_3$ (Panreac, > 97% purity) aqueous solutions, were circulated to the cell from the tanks by two peristaltic pumps (Watson Marlow 320, Watson Marlow Pumps Group) at $Q_l/A = 2$ ml min^{-1} cm^{-2}. The EC CO_2R measurements were undertaken at galvanostatic conditions ($j = 7.5$ mA cm^{-2}).

The MEA is the core of the Micro Flow Cell in the setup to perform the gas-phase EC CO_2R. It serves as the working electrode and separates the cathode and anode chambers, as shown in Fig. 3. To compare the influence of the cell configuration, the same abovementioned components (i.e., anode, membrane, reference) were employed to perform the test. In this configuration, a flow rate, Qg/A, of 18 ml min^{-1} cm^{-2} of pure CO_2 was fed to the cathode compartment, and a 0.5 M $KHCO_3$ aqueous solution was used as anolyte. The electrochemical measurements were accomplished at different galvanostatic conditions ($j = 5$, 7.5, 15, 30 and 40 mA cm^{-2}).

The electrochemical cells were operated at ambient conditions using an AutoLab PGSTAT 302 N potentiostat, controlling an overpressure at the outlet gas products stream. The gas product analysis was made using a four-channel micro gas chromatograph (3000 micro GC, Inficon). The volumetric CO_2 concentration in the outlet stream was above 98% in all the tests. This was considered in the selectivity calculations. The concentration of the products in the liquid phase was quantified after 50 min in a headspace gas chromatograph (GCMS-QP2010, Ultra Shimadzu) equipped with a flame ionisation detector (FID). An average concentration for liquid and gas samples was obtained

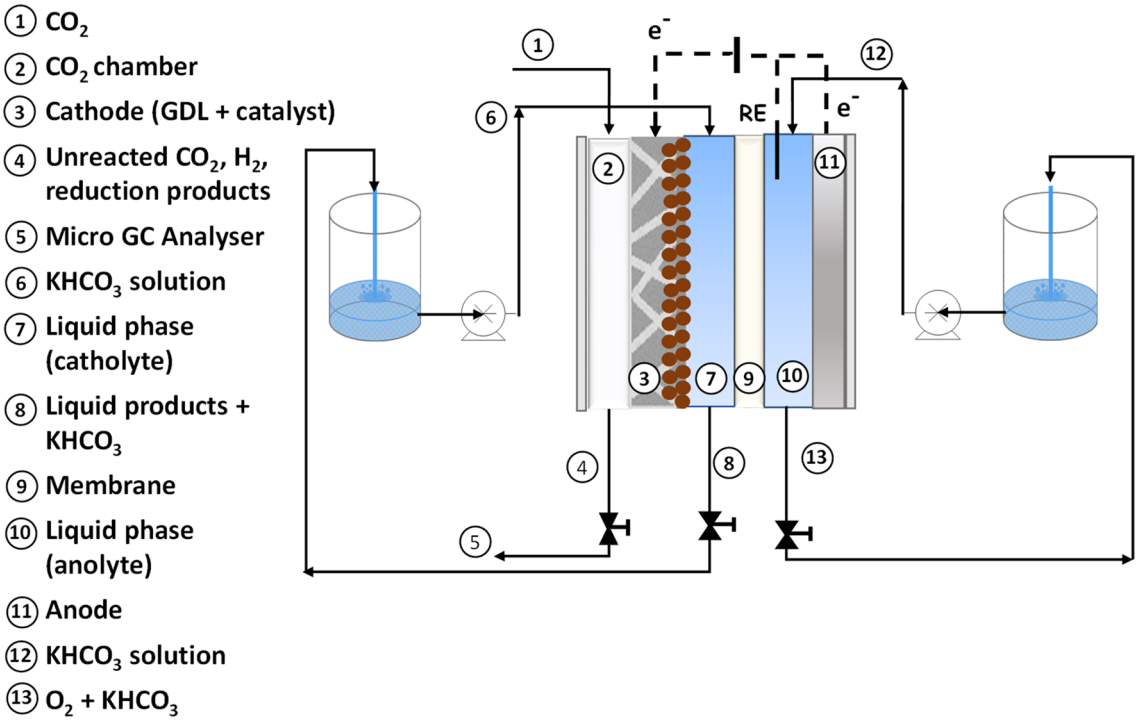

Fig. 2 Schematic layout of the GDE reactor configuration

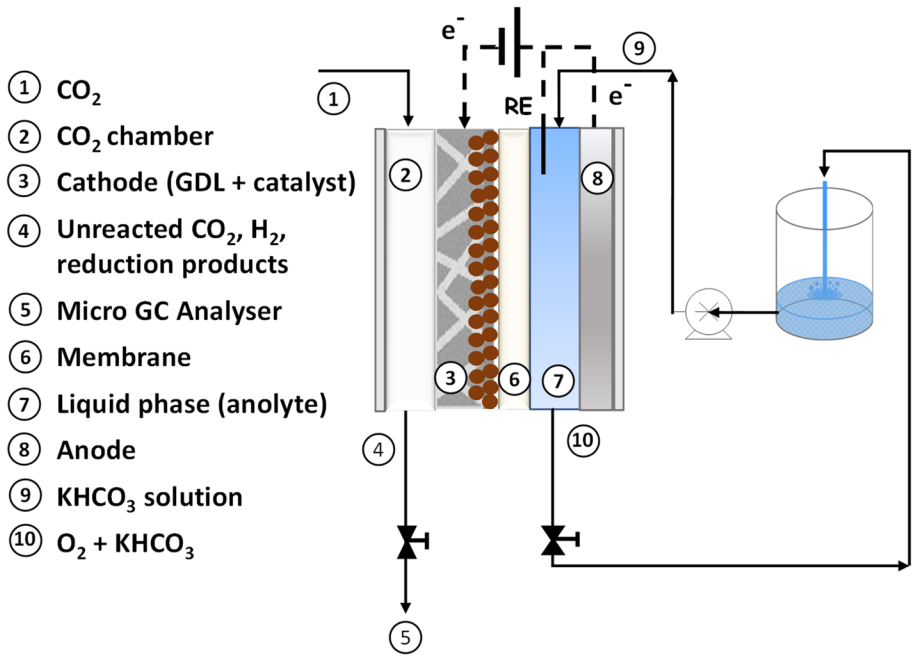

Fig. 3 Schematic layout of the MEA reactor configuration

for each point from the performance of three replicates. The maximum standard deviations for the replicates were lower than 14.5%.

The performance of the CO_2 reduction system is evaluated in terms of reaction rate, *r*, defined as the product obtained per unit of cathode area and time (in $\mu mol \cdot m^{-2} \cdot s^{-1}$); selectivity, *S*, defined as the ratio between the reaction rate for a specific product and the cumulative reaction rates for all products, and the faradaic efficiency, *FE*, which represents the efficiency at which electrons are transferred to form each product, according to the following equation:

$$FE(\%) = \frac{z \cdot n \cdot F}{q} \cdot 100 \quad (1)$$

where *z* is the theoretical number of e^- exchanged to form the desired product, *n* is the number of moles produced, *F* is the Faraday constant ($F = 96{,}485\ C \cdot mol^{-1}$), and *q* is the total charge applied.

2.3 Characterisation techniques

2.3.1 Field emission scanning *electron* microscopy (FESEM) with EDX

The information about the morphology and the content of the relative elements of the samples was obtained by using a ZEISS Supra 40 FESEM field emission scanning electron microscope (Oberkochen, Germany) equipped with an energy-dispersive X-ray spectroscopy system (EDS). It was operated at 3 kV. The samples were prepared by placing them onto a sample holder using conductive adhesive carbon tape before the FESEM analysis.

2.3.2 X-ray diffraction (XRD) analysis

XRD technique was operated to acquire information about the crystallinity of the samples by using a diffractometer (Panalytical X'Pert PRO) with monochromatic Cu-Kα radiation at 40 kV and 40 mA. XRD experiments utilised a PIXcel1D X-ray detector. The electrodes were scanned in grazing incident configuration with the X-ray source at a fixed 0.5° omega in the 2θ range of 25–80° with a scanning step of 0.020° and acquisition time of 8 s per step.

Table 2 Production rates (*r*) and selectivities (*S*) to hydrocarbons produced in the catholyte-less gas-phase MEA operation

Material	*E* (V vs. Ag/AgCl)	r (μmol·m^{-2}·s^{-1})						S_{CH4} (%)	S_{C2H4} (%)
		H_2	CO	CH_4	C_2H_4	CH_3OH	C_2H_5OH		
Cu-06	− 2.07	146.2 ± 9.4	44.8 ± 4.2	9.5 ± 0.3	27.3 ± 2.8	2.4 ± 0.3	3.1 ± 0.4	4.1	11.7
CuZ-06-3	− 1.76	243.3 ± 17.8	115.5 ± 13.7	11.3 ± 0.8	155.6 ± 13.2	0	Traces	2.1	29.6
CuZA-06-03-01	− 1.89	256.2 ± 12	88.8 ± 7.3	4.7 ± 0.3	99.2 ± 8	0	Traces	1	22.1

$j = 7.5$ mAcm^{-2}; $Q_g/A = 18$ mlmin^{-1} cm^{-2}

Traces of acetone were also detected

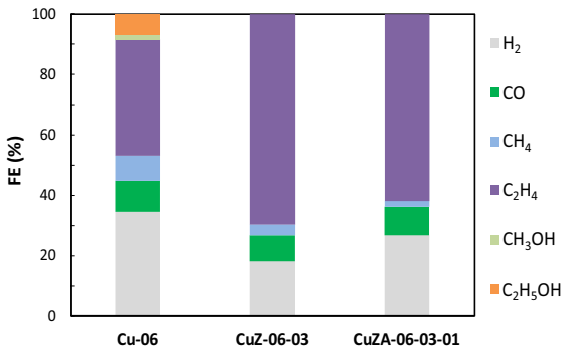

Fig. 4 FE as a function of the electrocatalytic material used in MEA operation. $j = -7.5$ mAcm^{-2}; $Q/A = 18$ mlmin^{-1} cm^{-2}

2.3.3 X-ray photoelectron spectroscopy (XPS) analysis

XPS measurements were conducted using a PHI 5000 Versa Probe (Physical Electronics) system. The instrument has a monochromatic X-ray source of 1486.6 eV (Al K-alpha) for determining the surface composition of the prepared materials. All core-level peak energies were referenced to the C1s peak at 284.8 eV, and the background signal, in high-resolution (HR) spectra, was detracted employing a Shirley function. The Multipak 9.7 software was used to complete the deconvolution procedure.

3 Results and discussions

3.1 Electrochemical measurements

3.1.1 Electrochemical CO_2 reduction in MEA and GDE configuration

Continuous CO_2 co-electrolysis tests under constant current density mode (chronopotentiometry) were performed to evaluate the ability of the CuZnAl-based electrodes to assist the EC CO_2R reaction. Table 2 and Fig. 4 show the main results for the continuous catholyte-less gas phase (MEA system) CO_2 reduction at a constant cathodic current density of 7.5 mA cm^{-2} as a function of the Cu-based investigated MEAs.

The results revealed a significant production of CO (r ~ 115 μmol m^{-2} s^{-1}) and C_2H_4 (r ~ 155 μmol m^{-2} s^{-1}) with the mixed-metal oxide (CuZ-06-03) electrode from the EC CO_2R reaction, as shown in Table 2. Additionally, CH_4 was also identified for all the Cu-based electrodes in operation. Lower rates for alcohols such as CH_3OH (r < 3 μmol m^{-2} s^{-1}) and C_2H_5OH (r < 4 μmol m^{-2} s^{-1}) were observed with a FE < 10% only with the Cu-06 electrocatalyst (see Fig. 4).

The investigated electrodes were demonstrated to be also active for the thermodynamically preferred HER under CO_2 conditions but with a lower FE than for the CO_2R (e.g., FE < 20% in the case of CuZ-06-03 electrode), as shown in Fig. 4. Indeed, the FE towards C_2H_4 was almost fourfold higher than the FEH_2 with the CuZ-06-03 electrode, which presents the lowest CuO crystallites in the fresh material and the highest ECSA (see section S1 and Figure S1 in the supporting information, SI). Figure 5 shows that the selectivity towards more reduced products (i.e., C_2H_4) seems to correlate with the ECSA value. In contrast, it is inversely proportional to the required electrode potential for each catalyst at the fixed applied current density (see Table 2), demonstrating a lower overpotential with the CuZ-06-03 electrode. Our results, in

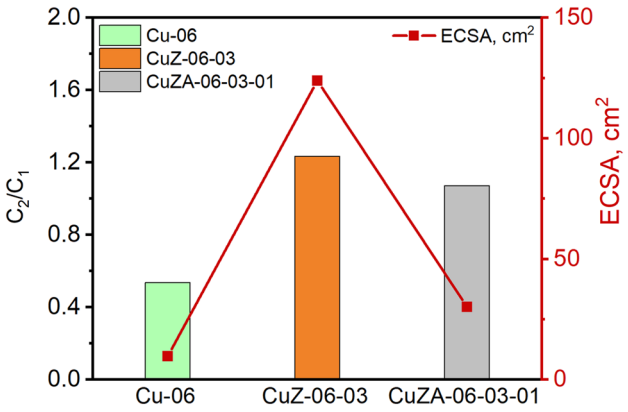

Fig. 5 Ratio between productivities towards C_2 and C_1 products, and the ECSA values as a function of the electrocatalysts used in MEA operation. $j = 7.5$ mAcm^{-2}; $Q/A = 18$ mlmin^{-1} cm^{-2}

catholyte-less conditions, suggest a size and electrochemically active sites-dependent selectivity for the CO_2R reaction and C_2 products in the MEA testing condition.

Three MEAs with the CuZ-06-03 catalyst were tested to assess the reproducibility of the significant results obtained with the zero-gap configuration. Figure 6 displays the time evolution of FE during the continuous production of H_2, CO, CH_4 and C_2H_4 through EC CO_2R reaction. Pretty steady-state conditions were achieved for the FE towards CO and CH_4 over 150 min of operation. In contrast, the FE towards C_2H_4 showed a decrease of up to 10% after 100 min, while the FE_{H2} increased. It could be related to the partial peel-off of catalyst particles from the electrode surface and the deactivation owing to the presence of concentrated CO_2 gas. The crystallisation of organic/inorganic substances and metal ions (e.g., K^+) from the anolyte on the electrode surface could further deteriorate the electrocatalytic activity [22]. Additional

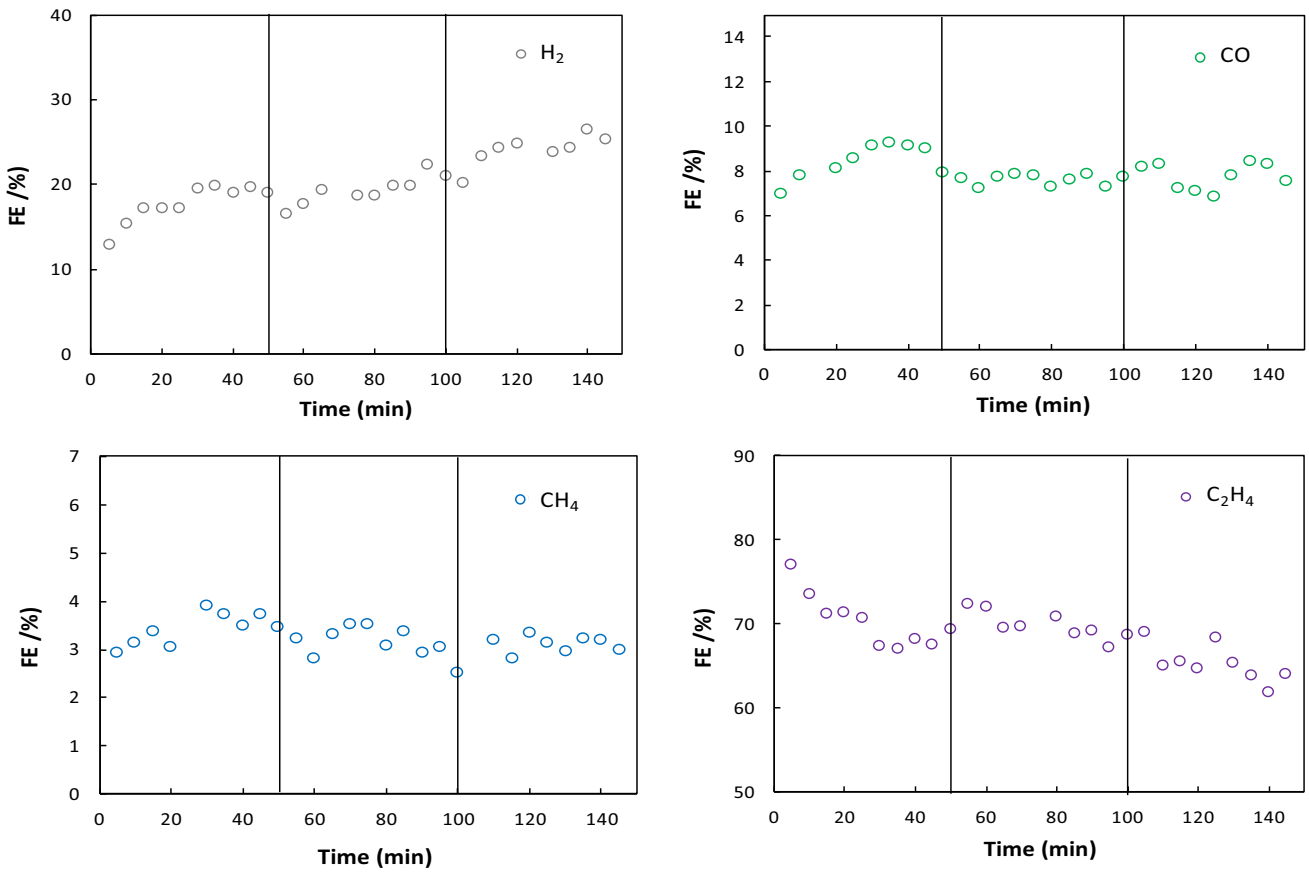

Fig. 6 Time dependence for FE towards H_2, CO, CH_4 and C_2H_4 at CuZ-06-03 after 3 consecutive runs in MEA operation. $j = -7.5$ mAcm^{-2}; $Q/A = 18$ mlmin^{-1} cm^{-2}

Table 3 Production rates (*r*) and selectivities (*S*) to alcohols and hydrocarbons produced in different operation modes (gas or liquid phase) using CuZ-06-03

Operation	*E* (V vs. Ag/AgCl)	*r* (μmol·m^{-2}·s^{-1})						S (%)			
		H_2	CO	CH_4	C_2H_4	CH_3OH	C_2H_5OH	CH_4	C_2H_4	CH_3OH	CH_5OH
MEA	− 1.76	243.3 ± 17.8	115.5 ± 13.7	11.3 ± 0.8	155.6 ± 13.2	0	Traces	2.1	29.6	0	0
GDE	− 1.45	215.5 ± 16.6	69.4 ± 6.9	5.2 ± 0.4	22.5 ± 1.4	55.4 ± 6.2	66.9 ± 8.8	1.2	5.2	12.7	15.4

$Q_g/A = 18$ mlmin^{-1} cm^{-2}; $Q_l/A = 2$ mlmin^{-1} cm^{-2}; $j = 7.5$ mAcm^{-2}

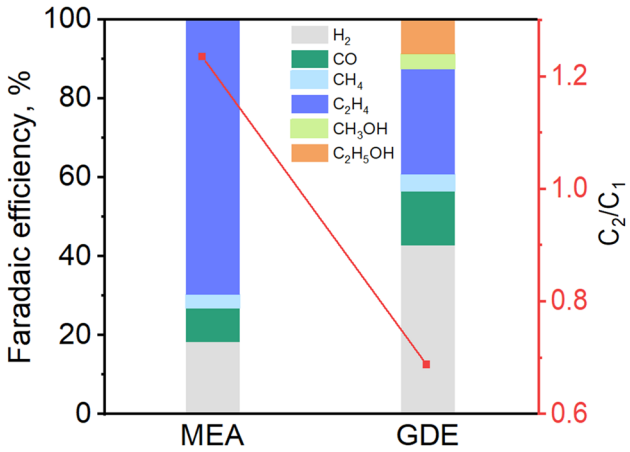

Fig. 7 FE and the ratio between productivities towards C_2 and C_1 products as a function of the operation mode (GDE and MEA) using CuZ-06-03; $Q_l/A = 18$ ml min^{-1} cm^{-2}; $j = 7.5$ mAcm^{-2}

experiments were carried out at different applied current densities to improve the EC CO_2R performance of the CuZ-06-03 electrocatalyst in the gas phase MEA system. Table S1 and Figure S2 in the SI show the results. It can be noticed that the productivity of H_2 gained importance when increasing the applied cathodic current density. That probably caused a high instability in the system due to the formation of many gas bubbles, involving a reduction in the selectivity towards C_2H_4 (from ~30% to ~5%).

The CuZ-06-03 GDE was then tested at the best j in the presence of bulk aqueous catholyte conditions (as shown in Fig. 2), achieving a different performance compared with the MEA in the catholyte-less gas-phase operation (see Fig. 3). The obtained values for the production rates of alcohols and hydrocarbons are listed in Table 3.

The FEs towards the different products from the EC CO_2R in the GDE system are displayed in Fig. 7. The performance is compared to that obtained in the MEA system. The results revealed that the investigated CuZ-06-03 electrode changed the reaction selectivity in the presence of the liquid phase electrolyte, showing a different product distribution. It could be attributed to the different catalyst reconstruction processes in the catholyte or catholyte-less testing conditions, generating different active sites with a determined electrocatalytic activity towards a specific product. Interestingly, the production rate, selectivity and FE for forming alcohol products increased with respect to the gaseous CO_2 reduction products in the presence of a liquid aqueous electrolyte, as shown in Fig. 7. However, the C_2/C_1 ratio and CO_2 conversion are higher in the gas phase MEA system than in the liquid electrolyte GDE configuration. The gas–solid–liquid three-phase interface generated in the GDE system promoted the formation of in-situ reactive species, enhancing the mechanism path involved in alcohol generation. Nevertheless, the CuZ-06-03 electrode showed a higher FE towards the hydrogen evolution reaction (~ 40%) under EC CO_2R in the GDE under liquid phase conditions than in the MEA system (see Fig. 7), as could be expected due to the higher amount of bulk water in the system.

The performance of the other Cu-based metal oxide catalysts (Cu-06 and CuZA-06-03-01) was also assessed in the GDE setup with the liquid catholyte. The results are shown in Table S2 and Figure S3 (in the SI). The reported production rates, selectivities, and FE of the generated products indicate that, for these catalysts, the selectivity towards alcohols was heightened in the presence of the liquid phase electrolyte. Indeed, the Cu-06 was the most-performing electrocatalyst to catalyse the CO_2 reduction reaction to alcohol products in the GDE system, which could be attributed to the CuO crystallites of the pristine materials.

Table 4 compares the total carbon productivities and the C_{2+}/C_{1+} ratios obtained during testing in the studied cell configurations for a proper interpretation of the electrocatalytic activity of the different materials. In agreement with

Table 4 Comparison of total carbon productivities and C_{2+}/C_{1+} ratios in MEA and GDE operation using the different Cu-based materials

Electrode	Configuration	Total carbons, μmol cm^{-2} s^{-1}	C_{2+}/C_{1+}	E, V vs. Ag/AgCl
Cu-06	MEA	87.10	0.54	− 2.07
	GDE	203.10	0.52	− 1.49
CuZ-06-03	MEA	283.40	1.24	− 1.76
	GDE	219.40	0.69	− 1.45
CuZA-06-03-01	MEA	193.70	1.07	− 1.89
	GDE	128.60	0.71	− 1.22

$j = 7.5$ mAcm^{-2}; $Q_g/A = 18$ ml min^{-1} cm^{-2}

the thermocatalytic process, the CO_2 reduction productivities into CuZ and CuZA catalysts increased in the catholyte-less EC configuration. Conversely, the MEA process significantly produces C_{2+} compounds instead of C_{1+} (i.e., methane, methanol, and CO), commonly produced at high T and P in the former process. However, it required an increasing applied voltage to maintain a stable cathodic current density (j = 7.5 mA cm^{-2}) with respect to the GDE process, which may be related to the fact that CO_2 is directly fed as gas to the cathodic compartment, provoking high resistances owing to the absence of catholyte. On the other hand, previous literature established that cations like K from the $KHCO_3$ catholyte facilitate the CO_2 activation step and the electron transfer process, which could explain the lower energy consumption in the presence of the liquid electrolyte [27].

3.2 Physico-chemical characterisation of CuZnAl-based electrodes

The FESEM micrographs of the pristine catalysts were described in detail in some of our previous work [21]. As mentioned in Sect. 2.1, the powders were deposited onto a conductive gas diffusion layer (GDL) by airbrushing the homemade catalytic ink to manufacture the cathodic electrodes. The in situ electrocatalyst reconstruction phenomenon could form different active sites that enhance the catalytic performance and determine catalyst selectivity. Therefore, the morphology and composition of the fresh and post-mortem electrodes were analysed to investigate their relationship with product distribution during the catalytic reaction. Figures 8a, c and e show high magnification FESEM images, which evidence the porous structures of the Cu-based materials in the fresh electrodes. In contrast, Fig. 8b, d and f confirm the electrocatalysts reconstruction after the EC CO_2R at a constant current density of − 7.5 mAcm^{-2} in MEA configuration (gas-phase operation). The micrograph of the Cu-06 tested electrode (Fig. 8b) shows sintered and agglomerate nanoparticles for the spherical hierarchical microstructures formed by porous pyramids in the fresh electrode, as shown in Fig. 8a. The EDS analysis of the post-mortem electrode in different zones resulted in a Cu/O atomic ratio of 1.07, like the pristine catalyst (1:1). Figure 8d evidences the modification of the CuZ-06-03 electrode after testing. The spherical surfaces (see Fig. 8c) were transformed into agglomerated random shapes constituted by Cu-enriched crystals in bulk with a relative Cu/Zn ratio of 80/60 determined by EDS. Figure 8f shows that the morphological changes were also evident in the case of the CuZA-06-03-01 electrode, which exhibits petals-like flake shapes, along with elongated crystals after the co-electrolysis of CO_2. Those flakes comprise Cu and Al-enriched crystals and amorphous structures, respectively, with a bulk Cu/Zn/Al molar ratio of 77:3:20.

As demonstrated above, the CuZ-06-03 electrode tested in the catholyte-less system exhibited a remarkable selectivity to C_2H_4 (see Sect. 3.1.1). It could be ascribed to the presence of nanocrystalline ZnO (crystallite size 7 nm) coupled with the small crystallite size of Cu-species (i.e. 7 nm CuO) in the fresh powder [21] that acted as CO-producing sites with an appropriate binding energy to stabilise the *CO intermediate for producing C_{2+} products [4, 28]. As aforementioned, the catalyst was also tested in the GDE configuration to compare the performance and evaluate the influence of the system in the catalyst reconstruction under the same operating conditions. For comparison, Fig. 9 shows the FESEM images that evidence the different morphological reconstructions of the catalyst under MEA and GDE operation. In particular, the original spherical structures were reconstructed into needle clusters and agglomerated tiny crystals in the GDE tested in the presence of the catholyte (see Fig. 9b) in contrast to the random particles formed in the gas phase MEA configuration, as shown in Fig. 9a. That result demonstrates that the cell configuration affects the catalyst reconstruction process.

The Cu2p doublet region of the CuZ-06-03 electrode acquired by XPS in HR mode of the tested samples, in MEA and GDE configurations, show a typical structure related to the mixed oxidation states of copper (Cu^0, Cu^{1+}, and Cu^{2+}). The deconvolution procedure of the Cu2p peak is complex because of the overlapping of the different Cu oxidation state

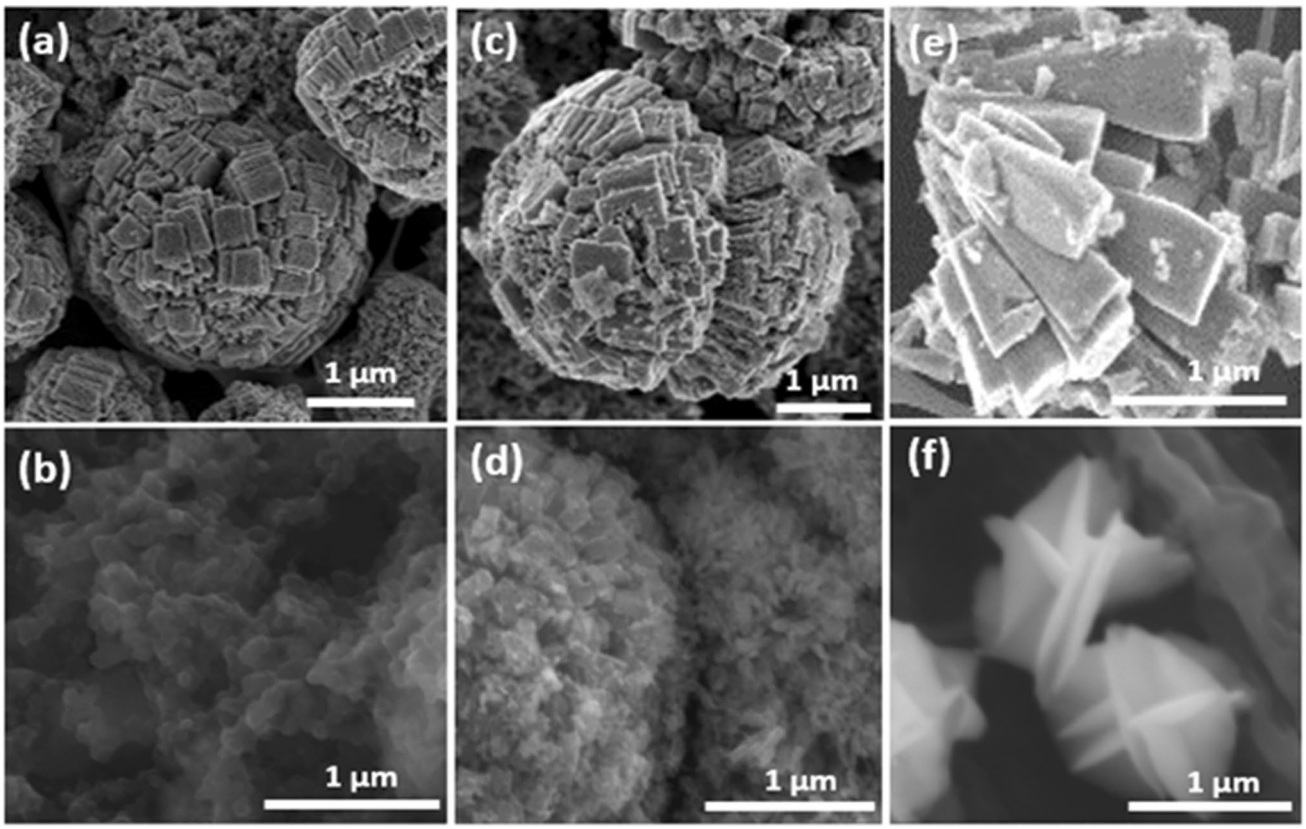

Fig. 8 FESEM micrographs of CuZnAl-oxide-based electrodes: Cu-06 (**a**) fresh and (**b**) tested; CuZ-06-03 (**c**) fresh and (**d**) tested; CuZA-06-03-0 1 (**e**) fresh and (**f**) tested. The electrodes were tested in catholyte-less gas phase MEA operation. $j = 7.5$ mAcm^{-2}; $Q_g/A = 18$ mlmin^{-1} cm^{-2}

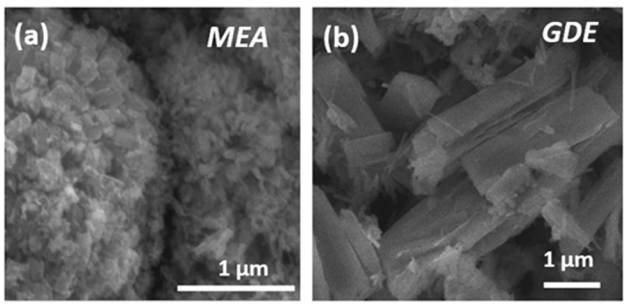

SAMPLES	Cu^{+2}	Cu^0+Cu^{+1}
CuZ-06-03_Fresh	92%	8%
CuZ-06-03_MEA	65%	35%
CuZ-06-03_GDE	72%	28%

Fig. 9 FESEM micrographs of CuZ-06-03 tested electrodes: **a** MEA and **b** GDE configuration. The table shows the percentage of oxidation states of copper on the catalyst surface calculated from XPS data. $j = 7.5$ mA cm^{-2}; $Q_g/A = 18$ mlmin^{-1} cm^{-2}, $Q_l/A = 2$ mlmin^{-1} cm^{-2}

binding energies. Therefore, the amount of Cu^{+2} and $Cu^0 + Cu^{+1}$ were approximated by fitting the $Cu2p_{3/2}$ peak and its related satellite employing the M. Biesinger et al. mathematical method (see Figure S4 in the SI) [29]. The table in Fig. 9 shows evidence that the kinetic of copper reduction under reaction is different in the investigated configuration cells, reaching a percentage of superficial $Cu^0 + Cu^{+1}$ four and three times higher than the fresh catalyst (8%) in the MEA and GDE systems, respectively. These results prove that the reduced copper, Cu^{+1}, and Cu^0 interface species at the electrode surface are the main active sites to improve the C–C coupling by *CO and *CH_x dimerisation reactions, the relative

amounts of which depend on the cell configuration. Indeed, the higher the $Cu^0 + Cu^{1+}$ percentage on the surface, the higher the FE to C_2H_4 (as shown from the results in Sect. 3.1.1).

The pristine nanoparticles present only the monoclinic CuO phase in the structure and hexagonal ZnO [21]. Figure 10 shows the XRD patterns of the tested CuZ-06-03 electrodes. The diffraction peaks in the XRD graph correspond to cubic Cu (JCPDS number: 00-04-0836), cubic Cu_2O (JCPDS number: 00-050-0667), hexagonal ZnO (JCPDS number: 00-036-1451) and Graphite (JCPDS number: 00-041-1487) crystalline phases. Some unknown peaks could be attributed to carbonate species deposited on the catalyst surface during the EC CO_2R. The ex-situ X-ray diffractogram demonstrates that the CuO oxidation state in the original catalyst was reduced to Cu^{+1} and Cu^0 under the employed CO_2 co-electrolysis conditions in both configurations. The semi-quantitative analysis revealed that after testing in GDE, the composition is approximately 36 wt% Cu, 41 wt% Cu_2O and 23 wt% ZnO. On the other hand, the post-mortem MEA electrode presents 70 wt% Cu, 10 wt% Cu_2O and 20 wt% ZnO. Those results indicate that the Cu^{+2} species (observed by the XPS analyses) are only present on the catalyst surface. Then, in the bulk, the Cu^{+1} in the cuprite (Cu_2O) crystallite size in the post-mortem GDE doubled from 7 to 16 nm, while the metallic Cu^0 formed crystallites of 8 nm and the ZnO crystallites of 10 nm. On the other hand, in the tested MEA, those phases formed larger crystallites. The Cu^0 crystallite size was 28 nm, whereas Cu^{+1} and ZnO presented crystallite sizes of 41 and 12, respectively. The crystallite size of each phase was calculated from the Debye–Scherrer equation. Those findings demonstrate that the smaller copper crystallite sizes possess higher selectivity for ethanol, which is in agreement with reported works that reveal that different edge site-to-face ratios play a crucial role in the selectivity of the reaction [30, 31]. It is further confirmed that the cell configuration influences the chemical composition and structure of the formed active sites, which lead to different activity and selectivity (i.e., alcohols or olefines) of the same pristine bimetallic catalyst, as demonstrated in Fig. 7.

3.3 Discussion

Copper attracts the most attention among the investigated catalysts in the EC CO_2R field. It is the most promising material for catalysing the CO_2 electrochemical reaction towards hydrocarbon and oxygenated compounds because it has a moderate affinity for *CO intermediate [32]. In thermocatalysis, amphoteric metal oxides (e.g. ZnO, Al_2O_3) were reported

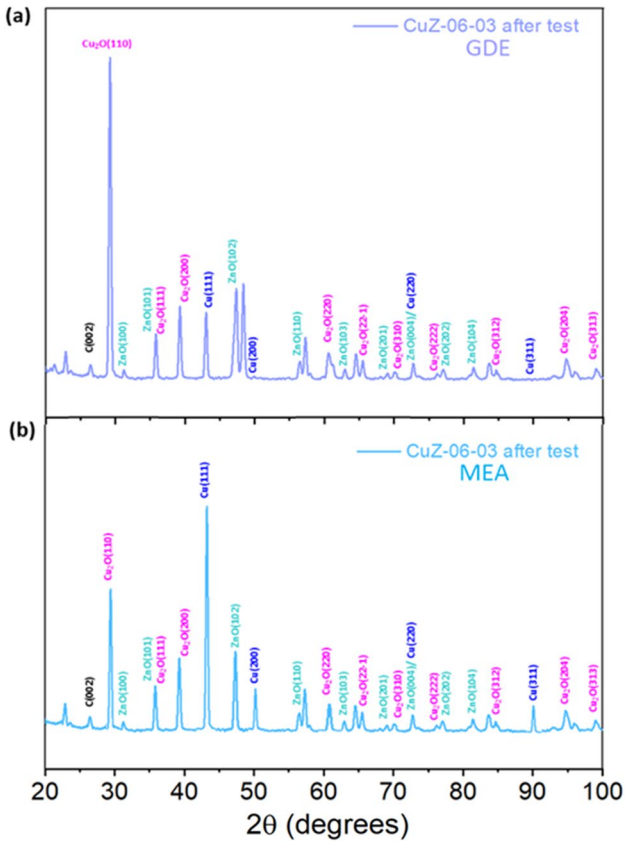

Fig. 10 XRD patterns of CuZ-06-03 electrodes tested in (**a**) GDE and (**b**) MEA system. $j = 7.5$ mA cm^{-2}

to increase the copper dispersion and surface area, inhibiting the sintering of the particles under operating conditions (H_2 atmosphere, high temperatures and high pressures). On the other hand, those metal oxides increase the basicity of the catalytic surface, favouring CO_2 adsorption, activation and further reduction. Herein, our results demonstrate that implementing those kinds of catalysts in the co-electrolysis of CO_2 in continuous-flow systems leads to the formation of promising chemicals, such as C_2H_4, which has a prominent growing market. Herein, copper oxidation states determined the reaction pathway to produce a specific product in the EC process. According to the literature, in the case of thermocatalysis, the Cu contained in the pristine catalyst is reduced entirely to metallic Cu^0 before the CO_2 reduction reaction at high T and P. Likewise, although the EC process is highly complex because other aspects influence the reaction (e.g. electrode polarisation, CO_2 availability), the electrocatalyst reconstruction during the reaction has been discovered even under ambient conditions. In this latter, most of the time, the electrocatalyst is partially reduced during testing. In particular, the here reported results prove that different amounts of Cu^{1+}/Cu^0 interfaces were formed on the CuZ-06-03 electrode according to the cell configuration implemented for the reaction. Ex-situ XRD characterisation analysis revealed that the percentage of Cu^0 (70 wt%) in bulk after testing in the MEA system was higher than the quantity generated during the test in the GDE configuration (36 wt%), which was further confirmed by XPS analysis. The different product distributions under MEA and GDE could be attributed to the improved covalent chemical bond of CO on Cu^{1+} cations with respect to metallic Cu surfaces. That is because of its decreased Cu 4 s/4p-derived density of states. Indeed, the CO desorption activation energy on Cu^0 surfaces (12–16 kcal/mol) is much lower than that of Cu^{1+} surfaces (i.e. 18.2–22.4 kcal/mol) [33], demonstrating that the abundant presence of Cu^0 surfaces on the catalyst leads to CO formation. Indeed, the outcomes shown in Table 3 indicate higher productivity towards CO in MEA than in the GDE configuration. Nevertheless, the selectivity towards C_2H_4 appears to be correlated with the CO formation. A small percentage of Cu^{1+}, besides Cu^0, on the catalyst in the MEA seems to generate an electrostatic tension between the two surface sites that promote the C–C coupling mechanism, favouring the dimerisation pathway for producing C_2H_4. This result agrees with previous research findings by Drisdell et al. [34] who assessed the selectivity towards multicarbon products of oxide-derived Cu catalysts tested in a MEA configuration. Operando X-ray absorption spectroscopy (XAS) measurements demonstrated that the C_2H_4 selectivity increased as Cu^0 increased on the catalyst surface. They stated that the amount of Cu^{1+} and Cu^{2+} oxide species after the reaction represents less than 10%. Similarly, Roldan B. et al. demonstrated through advanced operando X-ray studies that when the Cu catalyst structure is, on average, utterly metallic with a very thin layer of Cu^{1+}, the selectivity towards C_2H_4 increased during the EC CO_2R tests [35]. Conversely, the C_2H_4 formation was suppressed under liquid electrolyte conditions in the GDE configuration, whereas alcohols such as methanol and ethanol were boosted, as shown in Table 3. That could be ascribed to a balance between oxidised and reduced copper species on the catalyst surface that provides an optimal configuration between the CO adsorption energies on metallic and oxidised copper sites (stabilised by the ZnO presence), which are required for the C_2 oxygenated product formation [35]. Although our findings agree with those stated in literature employing operando characterisations, the authors are aware that copper species could reoxidise rapidly, which could compromise the accuracy of ex-situ methods for determining the real copper oxidation state of the catalyst during the EC CO_2R. Therefore, investigating the stability of Cu species in situ remains a challenge. Future research should investigate advanced in situ methods for examining the electronic structure of copper and tracking its valency on the catalyst surface while conducting electrochemical CO_2 reduction tests in different cells.

4 Conclusions

Cu–Zn-Al-based catalysts were tested for the EC CO_2R in the gas phase using a MEA catholyte-less setup and, for comparison, a GDE configuration with a liquid electrolyte. The reported results evidence that the type of operation and cell configuration remarkably impact the electrocatalytic activity, catalyst restructuration and, consequently, the product distribution using the same catalyst material. High C_2H_4 productivities were detected in gas phase operation from 5 to 40 $mA{\cdot}cm^{-2}$ using the MEA system, while this product was suppressed under liquid phase operation with the GDE system that instead boosted oxygenated compounds (i.e. CH_3OH and C_2H_5OH). This outcome remarks the effect of structure reconstruction and the crucial role of the copper oxidation states derived in situ during testing. Post-mortem characterisations in gas phase operation suggested that the electrochemical reduction conditions without bulk aqueous electrolytes promote a high Cu^0-content in the catalyst structure. In contrast, the morphological and chemical changes induced by the GDE operation induced an optimal balance between metallic copper and copper oxide species on the electrocatalyst, improving ethanol and propanol production. The detected dependency of the catalyst selectivity on the operation type of the EC CO_2R protocol provides prospects for steering the selectivity of the reaction on demand.

Further studies are required to achieve higher production rates and long-term stability, avoiding harsh electrolytes like KOH, previously used in the literature. Managing the degree of porosity and hydrophobicity in the electrode is critical to guarantee the appropriate transport of gases and prevent water accumulation (electrowetting phenomena due to water crossover from the anode) or K^+ deposition that could block the catalyst active sites.

Acknowledgements The authors acknowledge Mauro Raimondo for the FESEM measurements.

Author contributions Conceptualisation: SH; Methodology: HG, JA and SH; Electrochemical tests: JA; Formal analysis and investigation: HG, SH; XPS data analysis: MC; Writing -original draft preparation: HG; Writing—review and editing: SH, HG and JA; Supervision: AI; Funding acquisition: SH and JA; Resources: SH, JA, AI; All authors read and approved the final manuscript.

Funding SH acknowledge the financial support received from Fondazione Compagnia di San Paolo through the project CO_2Synthesis (ID ROL: 67910) funded in the Call Trapezio—Linea 1. J. A. fully acknowledge the financial support received from the Spanish State Research Agency (AEI) through the project TED2021-129810B-C21 (MCIN/AEI/https://doi.org/10.13039/501100011033 and Unión Europea Next Generation EU/PRTR).

Data availability The data that support the findings of this study are available on request from the corresponding author, SH.

Declarations

Competing interests The authors have no conflicts of interest in defining the content of this article.

References

1. da Cruz TT, Perrella Balestieri JA, de Toledo Silva JM, Vilanova MRN, Oliveira OJ, Ávila I. Life cycle assessment of carbon capture and storage/utilization: From current state to future research directions and opportunities. Int J Greenhouse Gas Control. 2021. https://doi.org/10.1016/j.ijggc.2021.103309.
2. Guzmán H, Salomone F, Batuecas E, Tommasi T, Russo N, Bensaid S, Hernández S. How to make sustainable CO_2 conversion to Methanol: Thermocatalytic versus electrocatalytic technology. Chem Eng J. 2021;417: 127973. https://doi.org/10.1016/j.cej.2020.127973.
3. Guzmán H, Russo N, Hernández S. CO_2 valorisation towards alcohols by Cu-based electrocatalysts: challenges and perspectives. Green Chem. 2021;23:1896–920. https://doi.org/10.1039/D0GC03334K.
4. Guzmán H, Salomone F, Bensaid S, Castellino M, Russo N, Hernández S. CO_2 conversion to alcohols over Cu/ZnO catalysts: prospective synergies between electrocatalytic and thermocatalytic routes. ACS Appl Mater Interfaces. 2022;14:517–30. https://doi.org/10.1021/acsami.1c15871.
5. Khoo HH, Halim I, Handoko AD. LCA of electrochemical reduction of CO_2 to ethylene. J CO2 Util. 2020;41:101229. https://doi.org/10.1016/j.jcou.2020.101229.
6. Precedence Research Ethylene Market Size 2022 To 2030. In: 2022. https://www.precedenceresearch.com/ethylene-market. Accessed 3 Jan 2023.
7. Samiee L, Gandzha S. Power to methanol technologies via CO_2 recovery: CO_2 hydrogenation and electrocatalytic routes. Rev Chem Eng. 2019;37:619–41. https://doi.org/10.1515/revce-2019-0012.
8. Guzmán H, Farkhondehfal MA, Rodulfo Tolod K, Russo N, Hernández S (2019) Photo/electrocatalytic hydrogen exploitation for CO_2 reduction toward solar fuels production. In: Solar Hydrogen Production Processes, Systems and Technologies. Elsevier Inc., p 560.
9. Dinh CT, Burdyny T, Kibria G, Seifitokaldani A, Gabardo CM, Pelayo GarcíaDeArquer F, Kiani A, Edwards JP, de Luna P, Bushuyev OS, Zou C, Quintero-Bermudez R, Pang Y, Sinton D, Sargent EH. CO_2 electroreduction to ethylene via hydroxide-mediated copper catalysis at an abrupt interface. Science (1979). 2018;360:783–7. https://doi.org/10.1126/science.aas9100.
10. Gabardo CM, O'Brien CP, Edwards JP, McCallum C, Xu Y, Dinh CT, Li J, Sargent EH, Sinton D. Continuous carbon dioxide electroreduction to concentrated multi-carbon products using a membrane electrode assembly. Joule. 2019;3:2777–91. https://doi.org/10.1016/j.joule.2019.07.021.
11. Li W, Yin Z, Gao Z, Wang G, Li Z, Wei F, Wei X, Peng H, Hu X, Xiao L, Lu J, Zhuang L. Bifunctional ionomers for efficient co-electrolysis of CO_2 and pure water towards ethylene production at industrial-scale current densities. Nat Energy. 2022;7:835–43. https://doi.org/10.1038/s41560-022-01092-9.
12. Gutiérrez-Guerra N, González JA, Serrano-Ruiz JC, López-Fernández E, Valverde JL, de Lucas-Consuegra A. Gas-phase electrocatalytic conversion of CO_2 to chemicals on sputtered Cu and Cu–C catalysts electrodes. J Energy Chem. 2019. https://doi.org/10.1016/j.jechem.2018.05.005.
13. Xia C, Zhu P, Jiang Q, Pan Y, Liang W, Stavitsk E, Alshareef HN, Wang H. Continuous production of pure liquid fuel solutions via electrocatalytic CO_2 reduction using solid-electrolyte devices. Nat Energy. 2019;4:776–85. https://doi.org/10.1038/s41560-019-0451-x.

14. Genovese C, Ampelli C, Perathoner S, Centi G. Electrocatalytic conversion of CO_2 on carbon nanotube-based electrodes for producing solar fuels. J Catal. 2013;308:237–49. https://doi.org/10.1016/j.jcat.2013.08.026.
15. Gutiérrez-Guerra N, Moreno-López L, Serrano-Ruiz JC, Valverde JL, de Lucas-Consuegra A. Gas phase electrocatalytic conversion of CO_2 to syn-fuels on Cu based catalysts-electrodes. Appl Catal B. 2016;188:272–82. https://doi.org/10.1016/j.apcatb.2016.02.010.
16. Gutiérrez-Guerra N, Valverde JL, Romero A, Serrano-Ruiz JC, de Lucas-Consuegra A. Electrocatalytic conversion of CO_2 to added-value chemicals in a high-temperature proton-exchange membrane reactor. Electrochem commun. 2017;81:128–31. https://doi.org/10.1016/j.elecom.2017.06.018.
17. García J, Jiménez C, Martínez F, Camarillo R, Rincón J. Electrochemical reduction of CO_2 using Pb catalysts synthesized in supercritical medium. J Catal. 2018;367:72–80. https://doi.org/10.1016/j.jcat.2018.08.017.
18. Gabardo CM, Colin P, Brien O, Jonathan P, Li J, Edward H, Sinton D, Brien CPO, Edwards JP, Mccallum C, Xu Y, Dinh C, Li J, Sargent EH, Sinton D. Continuous carbon dioxide electroreduction to concentrated multi-carbon products using a membrane electrode assembly continuous carbon dioxide electroreduction to concentrated multi-carbon products using a membrane electrode assembly. Joule. 2019;3:2777–91. https://doi.org/10.1016/j.joule.2019.07.021.
19. Hossain SKS, Saleem J, Rahman SU, Zaidi SMJ, McKay G, Cheng CK. Synthesis and evaluation of copper-supported titanium oxide nanotubes as electrocatalyst for the electrochemical reduction of carbon oxide to organics. Catalysts. 2019;9:1–19. https://doi.org/10.3390/catal9030298.
20. Álvarez A, Bansode A, Urakawa A, Bavykina AV, Wezendonk TA, Makkee M, Gascon J, Kapteijn F. Challenges in the greener production of formates/formic acid, methanol, and DME by heterogeneously catalyzed CO_2 hydrogenation processes. Chem Rev. 2017;117:9804–38. https://doi.org/10.1021/acs.chemrev.6b00816.
21. Guzmán H, Roldán D, Sacco A, Castellino M, Fontana M, Russo N, Hernández S. CuZnAl-oxide nanopyramidal mesoporous materials for the electrocatalytic CO_2 reduction to syngas: tuning of H_2/CO ratio. Nanomaterials. 2021;11:3052. https://doi.org/10.3390/nano11113052.
22. Albo J, Irabien A. Cu_2O-loaded gas diffusion electrodes for the continuous electrochemical reduction of CO_2 to methanol. J Catal. 2016;343:232–9. https://doi.org/10.1016/j.jcat.2015.11.014.
23. Merino-Garcia I, Albo J, Solla-Gullón J, Montiel V, Irabien A. Cu oxide/ZnO-based surfaces for a selective ethylene production from gas-phase CO2 electroconversion. J CO2 Util. 2019;31:135–42. https://doi.org/10.1016/j.jcou.2019.03.002.
24. Zeng J, Rino T, Bejtka K, Castellino M, Sacco A, Farkhondehfal MA, Chiodoni A, Drago F, Pirri CF. Coupled copper-zinc catalysts for electrochemical reduction of carbon dioxide. Chemsuschem. 2020;13:4128–39. https://doi.org/10.1002/cssc.202000971.
25. Merino-Garcia I, Albo J, Irabien A. Tailoring gas-phase CO_2 electroreduction selectivity to hydrocarbons at Cu nanoparticles. Nanotechnology. 2018;29:14001. https://doi.org/10.1088/1361-6528/aa994e.
26. Giusi D, Miceli M, Genovese C, Centi G, Perathoner S, Ampelli C. In situ electrochemical characterization of CuxO-based gas-diffusion electrodes (GDEs) for CO2 electrocatalytic reduction in presence and absence of liquid electrolyte and relationship with C_{2+} products formation. Appl Catal B. 2022;318: 121845. https://doi.org/10.1016/j.apcatb.2022.121845.
27. Salazar-Villalpando MD. Effect of electrolyte on the electrochemical reduction of CO2. ECS Trans. 2011;33:77–88. https://doi.org/10.1149/1.3565504.
28. Zhang T, Li Z, Zhang J, Wu J. Enhance CO_2-to-C_{2+} products yield through spatial management of CO transport in Cu/ZnO tandem electrodes. J Catal. 2020;387:163–9. https://doi.org/10.1016/j.jcat.2020.05.002.
29. Biesinger MC, Lau LWM, Gerson AR, Smart RSC. Resolving surface chemical states in XPS analysis of first row transition metals, oxides and hydroxides: Sc, Ti, V, Cu and Zn. Appl Surf Sci. 2010;257:887–98. https://doi.org/10.1016/j.apsusc.2010.07.086.
30. Loiudice A, Lobaccaro P, Kamali EA, Thao T, Huang BH, Ager JW, Buonsanti R. Tailoring copper nanocrystals towards C_2 products in electrochemical CO_2 reduction. Angewandte Chemie Int Edition. 2016;55:5789–92. https://doi.org/10.1002/anie.201601582.
31. Iyengar P, Kolb MJ, Pankhurst J, Calle-Vallejo F, Buonsanti R. Theory-guided enhancement of CO_2 reduction to ethanol on Ag- Cu tandem catalysts via particle-size effects. ACS Catal. 2021;11:13330–6. https://doi.org/10.1021/acscatal.1c03717.
32. Sun B, Dai M, Cai S, Cheng H, Song K, Yu Y, Hu H. Challenges and strategies towards copper-based catalysts for enhanced electrochemical CO_2 reduction to multi-carbon products. Fuel. 2023;332: 126114. https://doi.org/10.1016/j.fuel.2022.126114.
33. Cox DF, Schulz KH. Interaction of CO with Cu^+ cations: CO adsorption on Cu_2O(100). Surf Sci. 1991;249:138–48. https://doi.org/10.1016/0039-6028(91)90839-K.
34. Lee SH, Sullivan I, Larson DM, Liu G, Toma FM, Xiang C, Drisdell WS. Correlating oxidation state and surface area to activity from operando studies of copper CO electroreduction catalysts in a gas- fed device. ACS Catal. 2020;10:8000–11. https://doi.org/10.1021/acscatal.0c01670.
35. Timoshenko J, Bergmann A, Rettenmaier C, Herzog A, Arán-ais RM, Jeon HS, Haase FT, Hejral U, Grosse P, Kühl S, Davis EM, Tian J, Magnussen O, Cuenya BR. Steering the structure and selectivity of CO_2 electroreduction catalysts by potential pulses. Nat Catal. 2022;5:259–67. https://doi.org/10.1038/s41929-022-00760-z.